

Article pubs.acs.org/iournal/abseba

# Development of an N-Cadherin Biofunctionalized Hydrogel to Support the Formation of Synaptically Connected Neural Networks

Brian J. O'Grady, Kylie M. Balotin, Allison M. Bosworth, P. Mason McClatchey, Robert M. Weinstein, Mukesh Gupta, Kara S. Poole, Leon M. Bellan,\* and Ethan S. Lippmann\*



Cite This: ACS Biomater. Sci. Eng. 2020, 6, 5811-5822



**ACCESS** 

III Metrics & More

Article Recommendations

Supporting Information

ABSTRACT: In vitro models of the human central nervous system (CNS), particularly those derived from induced pluripotent stem cells (iPSCs), are becoming increasingly recognized as useful complements to animal models for studying neurological diseases and developing therapeutic strategies. However, many current three-dimensional (3D) CNS models suffer from deficits that limit their research utility. In this work, we focused on improving the interactions between the extracellular matrix (ECM) and iPSC-derived neurons to support model development. The most common ECMs used to fabricate 3D CNS models often lack the necessary bioinstructive cues to drive iPSC-derived neurons to a mature and synaptically connected state. These ECMs are also typically difficult to pattern into complex structures due to their mechanical

N-Cad peptide GelMA **Cell Death** Neurite **Projections** iPSC-derived Neuron Synaptogenesis

properties. To address these issues, we functionalized gelatin methacrylate (GelMA) with an N-cadherin (Cad) extracellular peptide epitope to create a biomaterial termed GelMA-Cad. After photopolymerization, GelMA-Cad forms soft hydrogels (on the order of 2 kPa) that can maintain patterned architectures. The N-cadherin functionality promotes survival and maturation of single-cell suspensions of iPSC-derived glutamatergic neurons into synaptically connected networks as determined by viral tracing and electrophysiology. Immunostaining reveals a pronounced increase in presynaptic and postsynaptic marker expression in GelMA-Cad relative to Matrigel, as well as extensive colocalization of these markers, thus highlighting the biological activity of the N-cadherin peptide. Overall, given its ability to enhance iPSC-derived neuron maturity and connectivity, GelMA-Cad should be broadly useful for in vitro studies of neural circuitry in health and disease.

KEYWORDS: induced pluripotent stem cell, hydrogel, biomaterial, neuron, neural network

# INTRODUCTION

Neurodegenerative diseases are estimated to affect 30 million people worldwide. Aging is the number one risk factor for neurodegeneration, and disease incidence is expected to increase concurrently with an increasingly aged population worldwide. These diseases (e.g., Alzheimer's disease, Parkinson's disease, Huntington's disease, amyotrophic lateral sclerosis, and multiple sclerosis) all have different regionspecific presentation and cell-cell communication, making it difficult to understand the mechanisms underlying their onset and propagation and thereby hampering the development of effective treatments. As an example, clinical trials for Alzheimer's disease have had a high failure rate since 2010 and currently available drugs can only alleviate symptoms but do not reverse neural tissue damage.2 These failures occur despite many candidate therapeutics having efficacy in various mouse models. As such, there has been a growing interest in developing human in vitro models for studying neurodegeneration<sup>3-8</sup> and reducing the attrition rate in therapeutic development.

Recent advancements in three-dimensional (3D) neural tissue models, particularly those constructed from human pluripotent stem cell (hPSC)-derived progenies (including human embryonic stem cells and induced pluripotent stem cells (iPSCs)), have generated much excitement for their ability to mimic the structure and function of human brain regions. 8-10 Such models typically consist of neurons and varying mixtures of supporting cells (e.g., glia and vascular components) embedded in a hydrogel formed from extracellular matrix (ECM) components. Currently, a wide variety of ECMs are available for constructing neural tissue models. Historically, the majority of early models have utilized Matrigel, an ECM composite derived from Engelbreth-Holm-Swarm mouse sarcoma tumors that consists of many

Received: June 11, 2020 Accepted: August 27, 2020 Published: August 27, 2020





proteins (type IV collagen, laminin, etc.) and growth factors. 12 For example, 3D Matrigel scaffolds have been used to support differentiation of mouse embryonic stem cells to neural cells.<sup>13</sup> Matrigel is also the predominant ECM utilized for more recently developed hPSC-derived brain organoids, 9,14 where the ECM scaffold supports the self-organization of the neuroepithelium to induce neuroepithelial buds and facilitates growth by providing a physical structure for the cells to attach and grow. 15 Other natural and synthetic materials have been developed for extended culture of hPSC-derived neural progenitor cells, (NPCs), neurons, and organoids, including silk, collagen, gelatin, hyaluronic acid (HA), elastin-like peptides, and polyethylene glycol (PEG).8,16-23 As these materials all allow for diffusion of essential nutrients and morphogens throughout the tissue constructs, they can be used to maintain NPCs and neuronal cultures for extended studies of differentiation and maturation, including axon formation, growth, and pruning. 17,24,25 Additionally, these platforms have demonstrated utility for assessing disease phenotypes when the hPSCs are sourced from patients that harbor genetic risk factors for each disorder. 16,1

Despite their utility toward fabricating complex neural tissue structures from hPSCs, existing ECMs have some known shortcomings for neural cell culture. Many ECM platforms lack appropriate bioinstructive cues to promote cell-cell or cell-ECM interactions that facilitate neuronal maturation. Of the aforementioned materials, only the components of Matrigel (e.g., laminin) and HA have physiological relevance to brain ECM; HA in particular has been shown to support hPSCderived NPC maturation into neurons that exhibit enhanced neurite projection with synaptic vesicles and electrophysiological activity.<sup>18</sup> However, Matrigel and HA are difficult to handle due to their viscosity, and both materials have a very low elastic modulus, meaning that they collapse under their own weight and cannot be molded into more complex macrostructures. These factors limit the fabrication of topographic features, such as vasculature or perfusion channels. Synthetic hydrogels may overcome these issues by incorporating custom functional groups that enable tuning of the mechanical and rheological properties, but they can be prohibitively difficult to fabricate and require more extensive chemical modification to recapitulate tissue-specific biochemical cell-ECM interactions.<sup>26</sup> Moreover, the majority of natural and synthetic ECMs are relatively expensive, which can further limit their widespread use.

Herein, we focused on engineering an ECM material to overcome some of these challenges. Our goal was to produce a material that would: (1) facilitate neuron survival and maturation within 3D tissue constructs through biophysical cues, (2) exhibit ideal mechanical properties to promote neuron outgrowth while also supporting macropatterned features, and (3) be relatively easy to synthesize at low cost and therefore widely accessible. We ultimately produced a biomaterial termed GelMA-Cad, which consists of methacrylated gelatin (GelMA, a well-characterized biomaterial capable of being photopatterned  $^{27-29})$  conjugated with a peptide from an extracellular epitope of N-cadherin (Cad) that has previously been used for cartilage tissue engineering.<sup>30</sup> Using this bioinstructive material, we form hydrogels with physiological stiffness that can not only maintain photopatterned features, but additionally facilitate iPSC-derived glutamatergic neuron survival and extension of neurite processes (as compared to GelMA, Matrigel, and various other negative

controls). Moreover, relative to Matrigel, GelMA-Cad supports enhanced formation of synaptically connected neural networks, as measured by immunocytochemistry, electrophysiology, and viral synaptic tracing. We suggest that GelMA-Cad will aid the construction of 3D neural tissue models to study human disease biology and augment drug screening assays.

## ■ MATERIALS AND METHODS

Cell Culture. CC3 iPSCs<sup>31</sup> were maintained in E8 medium on standard tissue culture plastic plates coated with growth-factor reduced Matrigel (VWR). At 60-70% confluency, the cells were passaged using Versene (Thermo Fisher) as previously described.<sup>32</sup> Cortical glutamateric neurons were generated using a previously described protocol<sup>33</sup> with some modifications. iPSCs were washed once with PBS and dissociated from the plates by incubation with Accutase (Thermo Fisher) for 3 min. After collection by centrifugation, the cells were replated onto Matrigel-coated plates at a density of 2.5  $\times$  10<sup>5</sup> cells/cm<sup>2</sup> in E8 medium containing 10  $\mu$ M Y27632 (Tocris). The following day, the medium was switched to E6 medium<sup>32</sup> supplemented with 10  $\mu$ M SB431542 (Tocris) and 0.4  $\mu$ M LDN1931189 (Tocris) for 5 days to induce neuralization as previously described.<sup>34</sup> Over the next 5 days, the media was gradually transitioned from E6 medium to N2 Medium (DMEM/F12 basal medium (Thermo Fisher) containing 1× N2 supplement (Gibco), 10  $\mu$ M SB431542, and 0.4  $\mu$ M LDN193189). <sup>34</sup> On the 11th day of the differentiation, the resultant neural progenitors were dissociated by incubation with Accutase for 1 h and passaged onto Matrigel in Neural Maintenance Medium with 10  $\mu$ M Y27632 at a cell density of  $1 \times 10^5$  cells/cm<sup>2</sup>. Neural Maintenance Medium was made by mixing a 1:1 ratio of N2 Medium and B27 Medium (Neurobasal Medium (Thermo Fisher) containing 200 mM Glutamax (Gibco) and 1× B27 (Gibco)). The cells received fresh Neural Maintenance Media every day for the next 20 days and a media change every 3-4 days afterward. Neurons were used for experiments between days 70 and 100 of differentiation.

For the synaptic tracing experiments described below, a small population of neurons was also transduced with an adeno-associated virus (AAV) encoding enhanced green fluorescent protein (EGFP) under the control of the human synapsin promoter, which was a gift from Dr. Bryan Roth (Addgene plasmid #50465). Two weeks before use, the neurons were dissociated with Accutase and replated onto Matrigel-coated plates at a density of 2.5  $\times$  10 $^{5}$  cells/cm $^{2}$  in Neural Maintenance Media containing 10  $\mu$ M Y27632. The following day, the media was replaced, and the AAV was added at a MOI of 5000. Fresh media was added to the cells after 24 h to remove any residual virus and normal media changes were resumed thereafter.

GelMA Synthesis and Characterization. Methacrylated gelatin (GelMA) was synthesized, as described previously.<sup>35</sup> Type A porcine skin gelatin (Sigma) was mixed at 10% (w/v) into DI water (sourced from an in-house Continental Modulab ModuPure reagent grade water system) at 60 °C and stirred until fully dissolved. Methacrylic acid (MA) (Sigma) was slowly added to the gelatin solution and stirred at 50 °C for 3 h. The solution was then centrifuged at 3500g for 3 min and the supernatant was collected. Following a 5× dilution with additional warm (40 °C) UltraPure water (Thermo Fisher) to stop the reaction, the mixture was dialyzed against DI water for 1 week at 37 °C using 12-14 kDa cutoff dialysis tubing (Fisher) to remove salts and MA. The pH of the solution was then adjusted to 7.35-7.45 by adding 1.0 M HCl or 1.0 M NaOH as measured with a Thermo Fisher Scientific Orion Star pH meter. The resulting GelMA solution was lyophilized for 3 days using a Labconco lyophilizer and stored at -20 °C.

**Peptide Conjugation and Characterization.** Peptides were conjugated to GelMA as previously reported<sup>30</sup> with slight modifications. Briefly, GelMA was reconstituted in triethanolamine (TEOA) buffer (Sigma) to create a 10% w/v solution and stirred at 37 °C for 2 h until fully dissolved. The pH of the solution was then adjusted to 8.0–8.5 by adding 1.0 M HCl or 1.0 M NaOH. Scrambled (Ac-AGVGDHIGC, to make GelMA-Scram) or N-cadherin mimic

(Ac-HAVDIGGGC, to make GelMA-Cad) peptides (GenScript) were added to the GelMA/TEOA buffer to form a 0.1% w/v solution. The cystine residue at the C-terminal end of the peptides permitted a Michael-type addition reaction with GelMA.<sup>30</sup> The solution was stirred at 37 °C for 24 h and then dialyzed against DI water using 6-8 kDa cutoff dialysis tubing (Spectrum) for 1 week at 37 °C. The pH of the solution was then adjusted to 7.35-7.45 by adding 1.0 M HCl or 1.0 M NaOH, and the solution was lyophilized and stored at -20 °C. Conjugation was routinely verified through <sup>1</sup>H-NMR using a Bruker 500 Hz NMR spectrometer set to 37 °C for the presence of the amino acid valine. The degree of functionalization of the methacrylic side chains to the gelatin backbone was determined by taking the integral of the lysine peak (~2.8-3.0 ppm) of gelatin and the GelMA spectra were normalized to the integral of the gelatin aromatic amino acid (~7.2-7.4) and then calculating the percent decrease in the lysine peak. 36,37 The degree of functionalization of the peptides to GelMA was calculated by normalizing the integral of the valine peak (~3.5 ppm) to the integral of the gelatin aromatic amino acid.

Fourier-Transform Infrared Spectroscopy. One hundred and ninety eight milligrams of potassium bromide (Sigma) was added to 2 mg of lyophilized gelatin, GelMA, GelMA-Cad, or GelMA-Scram and crushed using a mortar and pestle. The crushed samples were transferred to a 13 mm Specac evacuable pellet press die and compressed into a thin disc using a Specac manual hydraulic press. An additional disc was made using only potassium bromide for calibration. The samples were stored in a dry container overnight and analyzed the following day using a Bruker Tensor 27.

**Atomic Force Microscopy.** GelMA, GelMA-Scram, and GelMA-Cad were reconstituted and polymerized into hydrogel discs, as described in the cell seeding section below. A Bruker Dimension Icon Atomic Force Microscope was used to measure hydrogel stiffness. 0.01 N/m Novascan probes containing a 4.5  $\mu$ m polystyrene bead (PT.PS.SN.4.5.CAL) were used to measure three distinct 5 × 5  $\mu$ m<sup>2</sup> areas of each hydrogel. Three hydrogel disc replicates of each sample were utilized, with a total of 576 stiffness measurements per sample. For each individual force curve, a first-order baseline correction was performed, and the Hertzian model was used to calculate Young's modulus. For tool calibration, polyacrylamide hydrogels were prepared as previously reported<sup>38</sup> and measured prior to GelMA and its derivatives.

Rheological Characterization. The stiffness of GelMA, GelMA-Cad, and GelMA-Scram was measured using an AR-G2 (TA Instruments) strained-controlled rheometer equipped with 20 mm parallel plates. The hydrogels were loaded on the lower plate and photo-cross-linked for 8 s with 25 mW/cm² UV light using a ThorLabs UV Curing LED System. Immediately following UV exposure, the top plate was lowered to a gap of 0.8 mm. The cross-linking was recorded with a time sweep oscillatory test under constraint amplitude of 1% and at a constant frequency of 1 Hz. Three independent replicates were performed for each hydrogel condition.

**Scanning Electron Microscopy.** Lyophilized GelMA, GelMA-Cad, and GelMA-Scram were reconstituted in PBS to form 10% (w/v) solutions with a 0.05% lithium phenyl-2,4,6-trimethylbenzoylphosphinate (LAP) initiator (Sigma). Thirty microlitres of each hydrogel solution was added to a Ted Pella pin mount and cross-linked by an 8 s exposure to a 25 mW/cm² UV light. These pin mounts were stored in a Ted Pella mount storage tube and then placed in a -80 °C freezer overnight. The following day, the samples were transferred to a Labconco lyophilizer for an additional 2 days and then stored at room temperature until used. To characterize the internal microscructures of GelMA, GelMA-Cad, and GelMA-Scram, the dried samples were observed using a scanning electron microscope (Zeiss Merlin) at an accelerating voltage of 2 kV. ImageJ software was used to quantify pore sizes, where the mean diameter of each pore was considered the average pore size.

Fabrication and Seeding of Hydrogel Scaffolds. GelMA, GelMA-Scram, and GelMA-Cad were reconstituted in Neurobasal Medium to make a 10% (w/v) solution with a 0.05% LAP initiator. iPSC-derived neurons were detached from 12-well plates via a 5 min

incubation with Accutase and centrifuged for collection. The cells were mixed with a reconstituted hydrogel/initiator solution to achieve a density of  $2 \times 10^3$ ,  $2 \times 10^4$ , or  $2 \times 10^5$  cells/mL depending on the experiment. For experiments that assessed the influence of N-Cad peptide concentration, GelMA-Cad and GelMA were mixed to create a 2:1 ratio (66% GelMA-Cad concentration) and 1:2 ratio (33% GelMA-Cad concentration) and seeded with neurons at a density of 2 × 10<sup>5</sup> cells/mL. For some control experiments, GelMA was mixed with soluble peptide rather than via covalent coupling; here, soluble peptides were reconstituted in dimethyl sulfoxide (DMSO) to create a 10 mg/mL solution, and then the peptides were added to GelMA/ initiator/neuron solution (2 × 10<sup>5</sup> cells/mL) to create a 50  $\mu$ g/mL peptide concentration. Once the solutions were prepared, they were mixed thoroughly with a P1000 pipette to break up any cell clumps. Next, 100  $\mu$ L of the cell suspension was added to RainX-treated glass slides and covered with 12 mm diameter coverslips (Carolina) to form discs. These discs were then exposed to 25 mW/cm<sup>2</sup> UV light for 8 s and set aside for 10 min at room temperature. Hydrogel discs were then removed from the glass slides and transferred to a 12-well plate with 1 mL of Neural Maintenance Media per well.

To embed the neurons in Matrigel, 1 mL of Matrigel aliquots was thawed on ice. Once thawed, the neurons were embedded at a density of 2  $\times$   $10^{5}$  cells/mL, and 100  $\mu L$  of the solution was added directly onto the coverslips in a 12-well plate. The plate containing the Matrigel discs was placed in an incubator at 37  $^{\circ} C$  to cross-link for 30 min. After the Matrigel was fully cross-linked, 1 mL of Neural Maintenance Media was added to each of the wells.

For all experiments involving hydrogels, once the neurons were encapsulated, media was changed every 3 days until the cells were used.

**Live/Dead Cell Imaging.** To assess long-term cell viability, hydrogel discs were incubated with CytoCalcein Violet 450 (AAT Bioquest) and propidium iodide (PI, Thermo Fisher) for 1 h. This staining was performed at 48 h, 72 h, 5 days, and 10 days after embedding. The hydrogel discs were imaged using a Zeiss 710 confocal microscope and cell viability was quantified using ImageJ. Following imaging, 1 mL of Neural Maintenance Media was added to each well to dilute any remaining Calcein/PI from the hydrogels.

**Neurite Projection Quantification.** Raw data were exported in 16-bit TIF format and imported into MATLAB 2017 for quantification using a custom image analysis script. Briefly, the images were smoothed using a  $3\times3$  pixel smoothing filter to mitigate image noise, and in-focus neurite segments were identified by isolating the regions at least 5% brighter than the mean pixel intensity in the surrounding 50 pixel radius. <sup>39</sup> Cell bodies and neurites were distinguished by successive erosion of the resulting binary mass. The erosion radius at which the total cell mass declined most steeply was used to define the radius required to erode neurites while sparing cell bodies. Following segmentation of neurites and cell bodies, algorithms previously developed for analysis of the mitochondrial networks <sup>40</sup> were used to measure the average length and width of each neurite segment.

**Synaptic Tracing.** Hydrogel discs were fabricated as described above with wild-type neuron densities of  $2 \times 10^5$  cells/mL. Prior to cross-linking the hydrogels, separate neurons transduced with synapsin-driven EGFP were dissociated from plates via a 5 min incubation with Accutase and then added to the center of the hydrogel disc at a density of  $2 \times 10^3$  cells/mL (as shown in Figure 8). After cross-linking, the hydrogel discs were placed in 1 mL of Neural Maintenance Media and stored in an incubator at 37 °C until imaging. The formation of synaptic connections was visualized by the spread of EGFP fluorescence across the neuronal cultures using a Zeiss LSM 710 confocal microscope. On day 21, calcein was added to visualize live cells. Colocalization of EGFP and calcein was quantified using Zeiss Zen Black software.

**Immunofluorescence.** After 2 weeks of culture, the neurons embedded in hydrogels were fixed in 4% PFA (Sigma) for 20 min and then washed three times with PBS. A solution of 5% goat serum and 0.03% Triton X-100 (Thermo Fisher) was then added to the hydrogels overnight on a rocking platform at room temperature. The

Figure 1. Schematic illustration of gelatin methacrylate (GelMA) synthesis and N-cadherin peptide conjugation. The conventional method for synthesizing GelMA uses methacrylic anhydride (MA) to introduce a methacryloyl substitution group on the reactive primary amine group of amino acid residues. GelMA was then dissolved in TEAO buffer with the N-cadherin peptide for Michael-type addition to reactive primary amine groups.

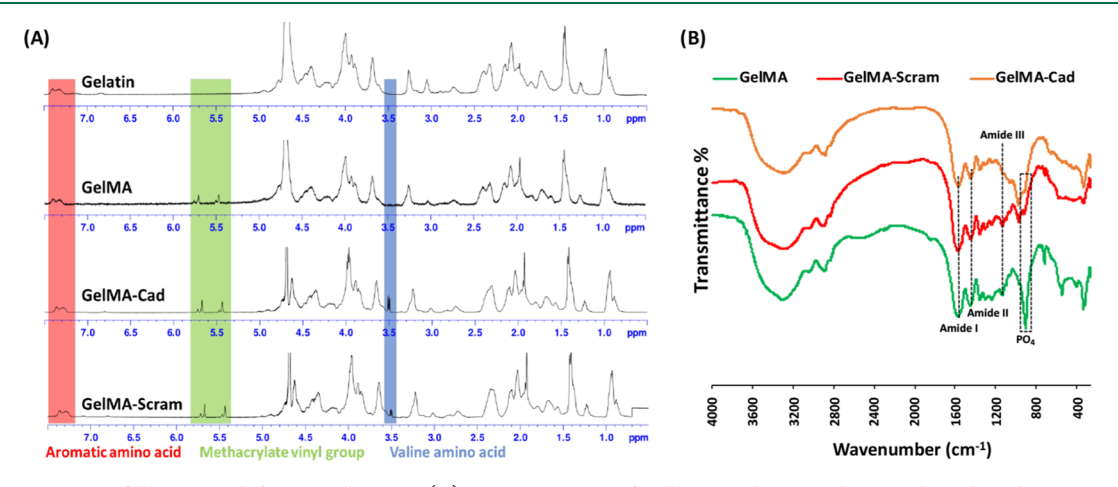


Figure 2. Assessment of biomaterial functionalization. (A) NMR spectra of gelatin, GelMA, GelMA-Cad, and GelMA-Scram. Successful conjugation of MA to the backbone of gelatin was assessed by peaks at 5.5 and 5.7 ppm, and N-cadherin/Scram peptide addition was assessed by the valine peak at 3.5 ppm. (B) FTIR spectra were used to confirm conjugation of the peptide to the backbone of GelMA due to decrease in the following relevant bands: 1000 cm<sup>-1</sup> (PO<sub>4</sub> stretching) and 1250, 1540, and 1640 cm<sup>-1</sup> (NH bending).

hydrogels were then incubated overnight with 4′,6-diamidino-2-phenylindole (DAPI) or fluorescently conjugated primary antibodies:  $\beta$ III tubulin Alexa Fluor 647 (Abcam ab190575), PSD-95 Alexa Fluor 488 (Novus Biologicals NB300556AF488), and/or synaptophysin Alexa Fluor 555 (Abcam ab206870). The hydrogels were then imaged using a 40× objective on a Zeiss LSM 710 confocal microscope. The number of PSD-95 and synaptophysin puncta was quantified using the cell counter plugin on ImageJ. Colocalization of the two markers was quantified using Zeiss Zen Black software.

**Electrophysiology.** The neurons embedded in GelMA-Cad or Matrigel hydrogels were recorded in a bath consisting of 140 mM NaCl, 2.8 mM KCl, 2 mM CaCl<sub>2</sub>, 2 mM MgCl<sub>2</sub>, 10 mM N-(2-hydroxyethyl)piperazine-N'-ethanesulfonic acid (HEPES), and 10 mM D-glucose. Sharp glass microelectrodes were prepared from borosilicate glass with a Sutter P97 pipette puller and filled with extracellular solution to reach a resistance of 6–8 MΩ. The recording electrode was placed near the edge of the hydrogel disc. Extracellular field potential recordings were performed in a recording chamber placed on the stage of a Zeiss Axioscope upright microscope. The electrical activity was recorded with an Axon Multiclamp 700A amplifier. Data recording and analysis were performed with Axon pClamp software.

# **■ RESULTS**

Synthesis and Characterization of GelMA Functionalized With N-Cadherin Peptide. GelMA was chosen as a base material due to its ease of handling and robust mechanical

properties (after cross-linking) compared to ECMs such as Matrigel and HA. Meanwhile, N-cadherin functionality was chosen for the role of this cell adhesion molecule in neurite growth during neurogenesis. The extracellular peptide epitope of N-cadherin chosen for this study has previously been used to functionalize methacrylated HA to support chondrogenesis from mesenchymal stem cells, but 3D scaffolds fabricated with this peptide have not been used to support neural cultures. To generate the GelMA-Cad scaffold, porcine gelatin was first functionalized with methacrylic anhydride to create the GelMA backbone that could be cross-linked when exposed to the photoinitiator LAP and UV light (Figure 1).

This modification was confirmed through the presence of methacrylic side-chain protons ( $\sim$ 5.45 and 5.7 ppm) using  $^1\text{H-NMR}$  (Figure 2A), where a 77.5  $\pm$  8.4% degree of functionalization was achieved. GelMA was then functionalized with the extracellular epitope of N-cadherin (HAVDIGGGC) or an N-cadherin-scrambled peptide (AGVGDHIGC), which is referred to as GelMA-Scram. The conjugation of these peptides to the scaffold was also confirmed via  $^1\text{H-NMR}$  through the presence of valine protons ( $\sim$ 3.5 ppm), which are not present in the gelatin or GelMA spectra (Figure 2A). Based on the NMR spectra, 39.4  $\pm$  12.7 and 38.2  $\pm$  19.2% degrees of functionalization were achieved for GelMA-Cad and GelMA-

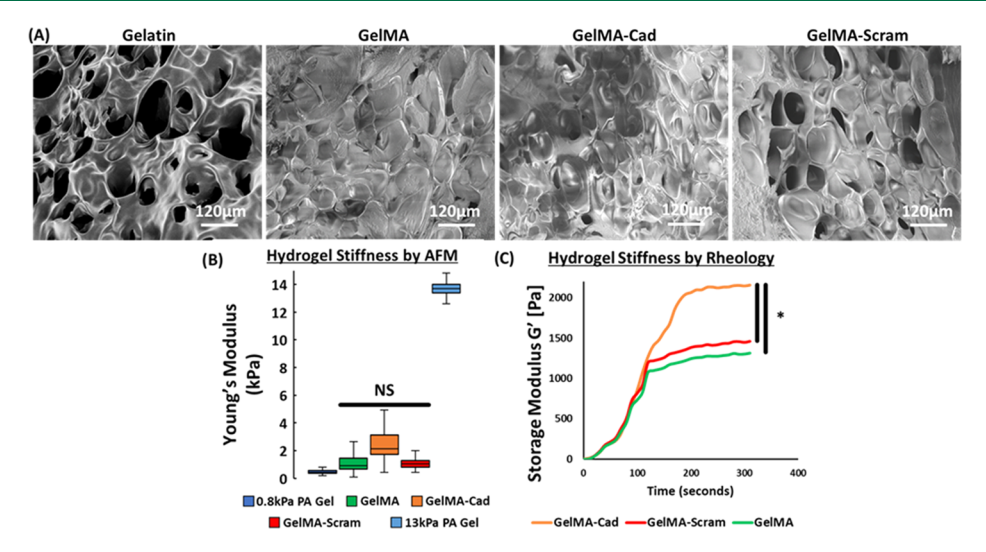


Figure 3. Physical properties and cross-linking kinetics of the hydrogels characterized using SEM, AFM, and rheology. (A) SEM images of the hydrogels fabricated from gelatin, GelMA, GelMA-Cad, and GelMA-Scram. (B) AFM measurements of Young's modulus values for GelMA, GelMA-Cad, and GelMA-Scram. Stiffness data in the main text are presented as mean  $\pm$  standard deviation (SD) from 3 individually prepared hydrogels. Statistical significance was calculated from one-way analysis of variance (ANOVA) with Tukey's post hoc test (NS = not significant). (C) Cross-linking kinetics of GelMA, GelMA-Scram, and GelMA-Cad evaluated by rheology. Stiffness data from the 300 s endpoint are presented in the main text as mean  $\pm$  SD from 3 individually prepared hydrogels. Statistical significance was calculated using unpaired Student's t-test calculations between GelMA-Cad and the two control hydrogels (\*p < 0.0001).

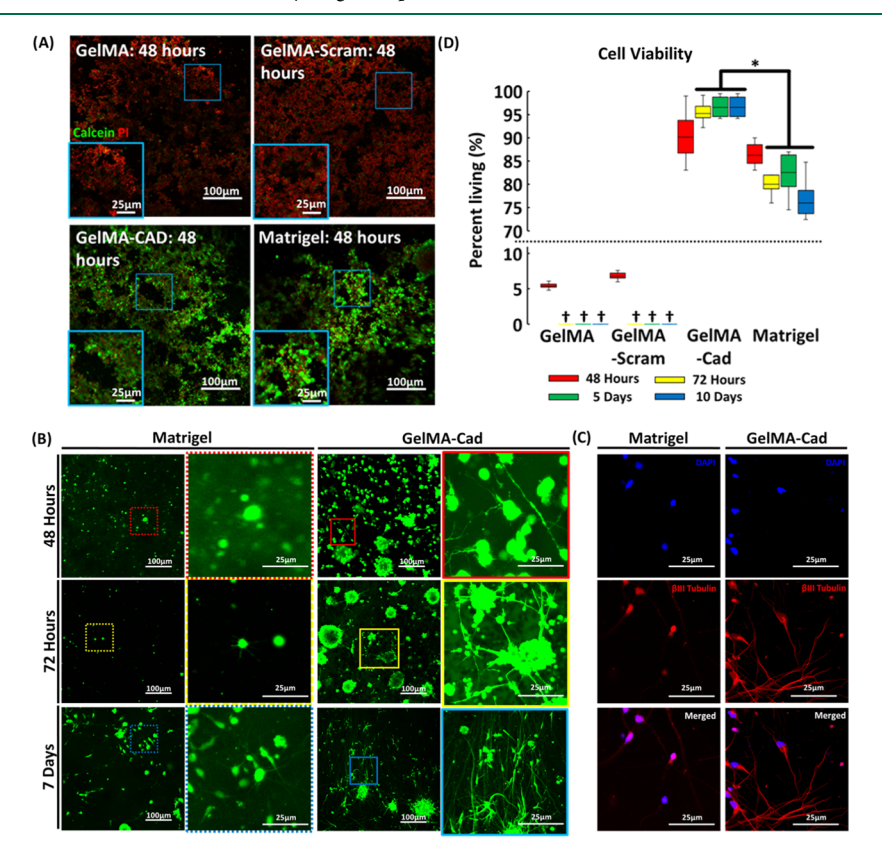


Figure 4. Live/dead staining of the iPSC-derived neurons embedded in various hydrogels. (A) Representative images of the hydrogels that were labeled after 48 h with calcein (green) and propidium iodide (PI, red) to visualize the live and dead cells, respectively. The insets are provided for higher magnification. (B) Representative images of Matrigel and GelMA-Cad hydrogels labeled at various time points with calcein. The insets are provided for higher magnification. (C) Neurons in Matrigel and GelMA-Cad were immunolabeled with  $\beta$ III tubulin (red) and DAPI (blue) to confirm identity and morphological observations. (D) Full quantification of cell viability, using calcein and PI, for all conditions and time points. Data are presented as mean  $\pm$  SD from three biological replicates, with five images assessed per replicate.  $\dagger$  is used to highlight values that fall below 5%. Statistically significant differences in the viability were calculated between GelMA-Cad and Matrigel at later time points using a one-way ANOVA with Tukey's post hoc test (\*p < 0.005).

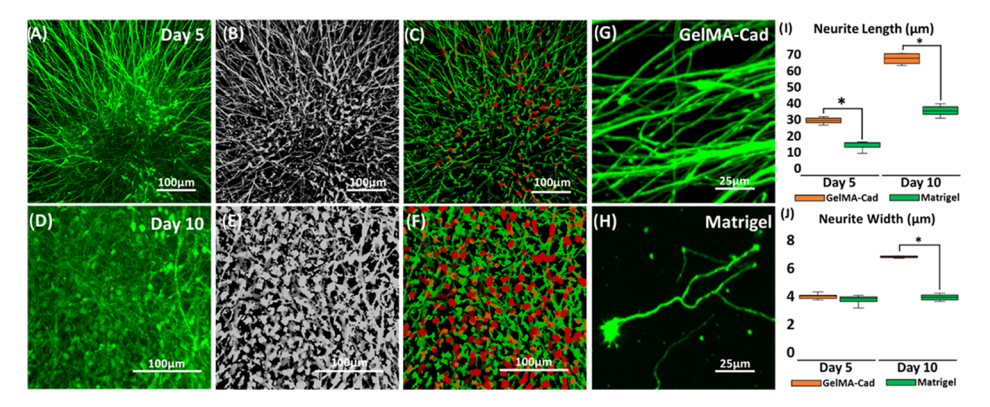


Figure 5. Quantification of the neurites in the iPSC-derived neurons embedded in Matrigel and GelMA-Cad. Panels A–C demonstrate the quantification of the neurites in GelMA-Cad on day 5, and panels D and E demonstrate the quantification of the neurites in GelMA-Cad on day 10. The neurons are stained with calcein (green) and imaged with a confocal microscope (A, D). Using custom MATLAB code as described in ref 40, a mask is applied (B, E) and cell soma and neurites are identified (C, F), where red corresponds to the soma and green corresponds to neurite extensions, which can then be measured and averaged across an image. (G, H) Example of high-resolution images of the neurites in GelMA-Cad and Matrigel, where differences in neurite length and thickness can be observed. (I, J) Full quantification of neurite length and width. Data are presented as mean  $\pm$  SD from seven biological replicates, with four images quantified per biological replicate. Statistical significance was calculated using the Student's unpaired t-test (\*p < 0.05).

Scram, respectively. Additionally, Fourier-transform infrared (FTIR) spectroscopy was employed to further validate successful functionalization. The FTIR transmittance spectra showed a noticeable decrease in the PO<sub>4</sub> peaks (1000 cm<sup>-1</sup>) and amide peaks I, II, III (1640, 1540, and 1250 cm<sup>-1</sup>, respectively) in the GelMA-Cad and GelMA-Scram samples compared to GelMA (Figure 2B), likely due to peptide conjugation. Collectively, these data suggest that GelMA was properly synthesized and functionalized.

Mechanical and Physical Properties of Cross-linked Hydrogels. The microporous structures of cross-linked hydrogels were confirmed by scanning electron microscopy (SEM). Porous network structures are commonly observed in hydrogels and are important for nutrient diffusion, cell integration, and removal of waste products, and the degree of chemical substitution has an inverse relation to pore size upon cross-linking.<sup>22,47</sup> The average pore size diameters of GelMA, GelMA-Cad, and GelMA-Scram were measured at  $42.8 \pm 0.2$ ,  $43.1 \pm 0.2$ , and  $42.4 \pm 0.2 \mu m$ , respectively (Figure 3A). Next, to determine the local stiffness of GelMA, GelMA-Cad, and GelMA-Scram, atomic force microscopy (AFM) was performed. Polyacrylamide hydrogels (0.8 and 13 kPa) were produced and measured by AFM<sup>38</sup> to validate that the tool was properly calibrated (Figure 3B). After cross-linking with LAP and UV light, GelMA, GelMA-Cad, and GelMA-Scram exhibited stiffness values of approximately 1-5 kPa (Figure 3B), which resembles the stiffness of the native brain tissue. 48,49 Despite its relatively low elastic modulus, GelMA-Cad is stiff enough to maintain patterned architectures: when it was cross-linked around silicone tubing, followed by manual extraction of the tubing, a straight, a perfusable channel remained in the GelMA-Cad (Figure S1A), whereas Matrigel collapses and the perfusion channel does not remain patent (Figure S1B). Thus, similar to GelMA, 35,50 GelMA-Cad can be patterned into more complex macrostructures. To determine bulk stiffness, cross-linked hydrogels were measured by rheometry, where the stiffness of GelMA, GelMA-Scram, and GelMA-Cad was determined to be  $1.3 \pm 0.03$ ,  $1.4 \pm 0.03$ , and  $2.1 \pm 0.04$  kPa, respectively (Figure 3C). Overall, the average local and bulk stiffness measurements are in good agreement, and these measurements confirm that the hydrogels all have

similar physical and mechanical properties, such that differences in neuron behavior can likely be attributed to peptide functionalization.

GelMA-Cad Hydrogels Support Survival and Outgrowth of iPSC-Derived Neurons. To assess the ability of the hydrogels to support human neuron survival and outgrowth, human iPSCs were differentiated into highly pure populations of cortical glutamatergic neurons and cultured for 70-100 days before use. This early time point was chosen to ensure that the neurons were relatively immature, such that the effects of hydrogel encapsulation on maturation could be more easily judged. Furthermore, the neurons were dissociated into single-cell suspensions rather than more commonly used aggregates so that we could better assess the effects of hydrogel encapsulation on survival. The neurons were first embedded into Matrigel, GelMA-Cad, GelMA-Scram, or GelMA. As a negative control for physical conjugation of the peptides to the hydrogels, the neurons were also embedded in GelMA with either soluble N-cadherin peptide or soluble scrambled peptide. Using calcein and propidium iodide dyes to mark live and dead cells, respectively, we determined that neurons embedded in GelMA and GelMA-Scram (both conjugated and soluble peptide), as well as Matrigel with the soluble peptide, died within 4 days (Figures 4A and S2). Meanwhile, the neurons in conjugated GelMA-Cad and Matrigel exhibited the viability of 90.2  $\pm$  1.3 and 86.3  $\pm$  2.2% after 2 days, respectively (Figure 4B). After 3 days, the neurons in conjugated GelMA-Cad exhibited the viability of 96.7  $\pm$ 1.2%, while the viability in Matrigel decreased slightly to 80  $\pm$ 1.3% (Figure 4B). After 5 days, the viability remained relatively constant (96.7 ± 1.1% in conjugated GelMA-Cad versus 82.3 ± 1.9% in Matrigel), and by day 10, the viability in conjugated GelMA-Cad continued to remain constant at 96.7 ± 1.6%, whereas the viability in Matrigel again decreased slightly to 76.7  $\pm$  0.8% (Figure 4B).  $\beta$ III tubulin immunolabeling is shown in Figure 4C to confirm neuron identity and full quantifications are shown in Figure 4D.

Next, we monitored neurite projections from single-cell suspensions of the neurons embedded in either Matrigel or conjugated GelMA-Cad (referred to solely as GelMA-Cad from hereon) after 5 and 10 days using calcein. Neurite length

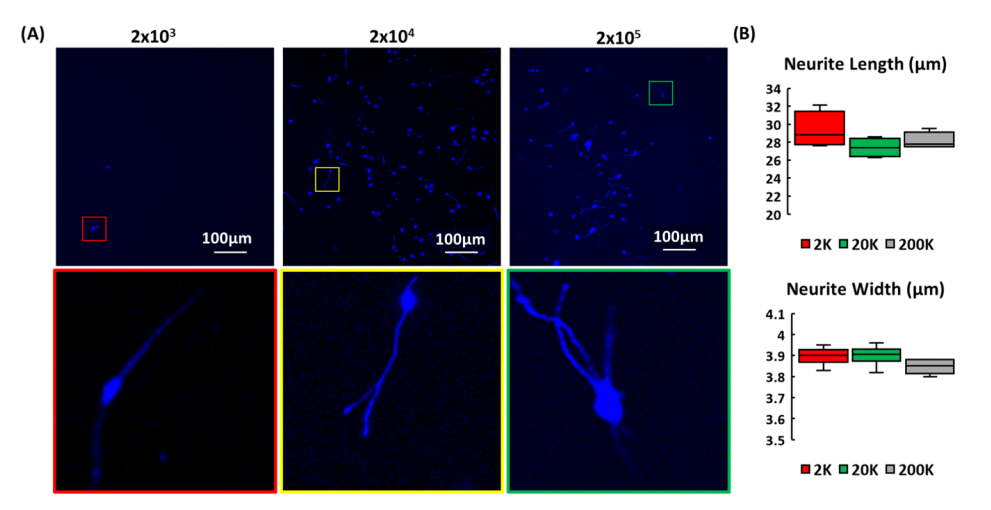


Figure 6. Influence of cell density on the neuron physical properties in GelMA-Cad. (A) Representative images of the calcein-labeled neurons embedded in GelMA-Cad hydrogels at various cell densities. The numbers above each figure are the corresponding density (cells/mL). The scale bar is the same for all images. An inset is provided to highlight the morphology for each density. (B) Quantification of neurite length and width. Mean  $\pm$  SD was calculated from three biological replicates, with two confocal z-stack images (200  $\mu$ m depth) assessed per replicate. No significant differences were measured as calculated using a one-way ANOVA with Tukey's post hoc test.

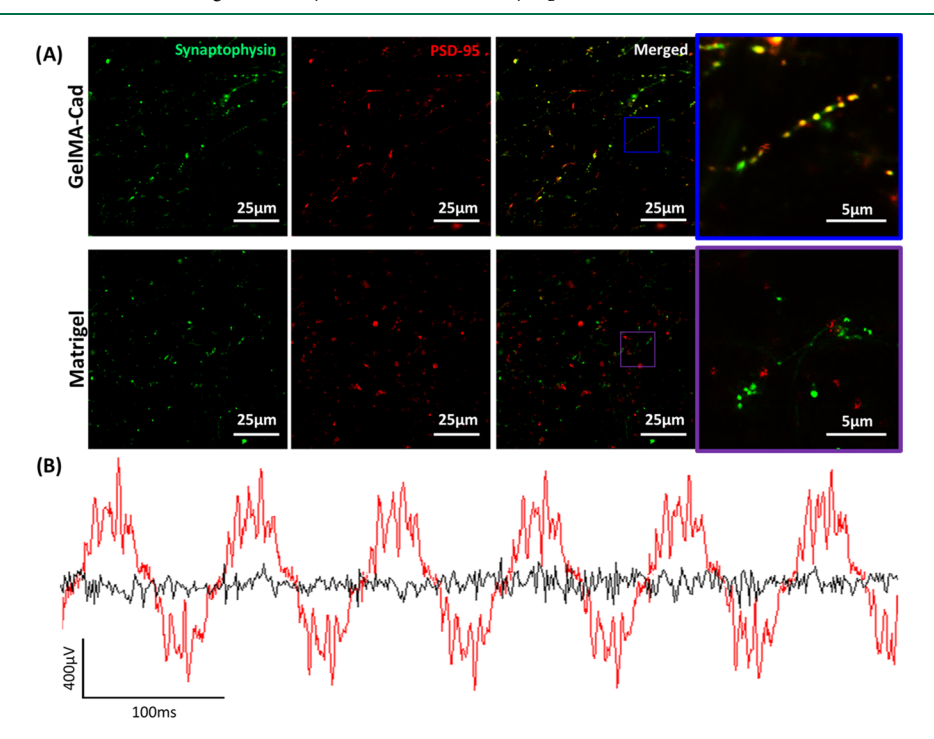


Figure 7. Assessment of synaptic connectivity of the iPSC-derived neurons in Matrigel or GelMA-Cad by immunostaining and electrophysiology. (A) Immunostaining of synaptophysin (green) and PSD-95 (red) in the neurons that were embedded in each hydrogel for 21 days. An inset is provided to highlight pronounced differences. Ten images from three biological replicates were used for quantification, and statistical significance was calculated using the Student's unpaired *t*-test. (B) Extracellular field potential measurements for the neurons embedded in GelMA-Cad (red) and Matrigel (black) for 21 days. Voltage traces are representative of 5 biological measurements.

and width are frequently employed as measures of neuron health and connectivity,  $^{51-55}$  and so we quantified Z-stack images of neurites using a custom MATLAB script. On day 5, relative to Matrigel, individual neurons embedded in GelMA-Cad exhibited significantly higher average neurite length (28.9  $\pm$  1.6 vs 14.1  $\pm$  2.6  $\mu$ m; p < 0.05), whereas average neurite width was not significantly different between GelMA-Cad and Matrigel (4.0  $\pm$  0.2 vs 3.7  $\pm$  0.2  $\mu$ m) (Figure 5). However, on day 10, relative to Matrigel, individual neuron in GelMA-Cad exhibited significantly higher average neurite

length (67.2  $\pm$  3.2 vs 35.3  $\pm$  7.1  $\mu$ m; p < 0.05) and average neurite width (6.8  $\pm$  0.2 vs 3.9  $\pm$  0.2  $\mu$ m; p < 0.05).

To determine if peptide concentration in the hydrogel affected neurite width and length, the cells were embedded in a 2:1 ratio hydrogel of GelMA-Cad/GelMA (66%) and 1:2 GelMA-Cad/GelMA (33%) (Figure S3A–B). After 5 days, the cells were stained with calcein and again quantified for neurite length and width. In the 66% GelMA-Cad/GelMA hydrogels, the average neurite length and width were not significantly different compared to the average neurite length and width in the GelMA-Cad hydrogels (24.7  $\pm$  2.1 and 3.9  $\pm$  0.2  $\mu m$ )

(Figure S3C-D). However, the cells embedded in 33% GelMA-Cad/GelMA hydrogels exhibited significantly lower average length (17.5  $\pm$  2.4  $\mu$ m; p < 0.05), whereas the average neurite width was not significantly different from the GelMA-Cad and 66% hydrogels  $(3.8 \pm 0.3 \mu m)$  (Figure S3C-D). To determine if cell density affected behavior in the hydrogel, seeding densities of  $2 \times 10^3$ ,  $2 \times 10^4$ , and  $2 \times 10^5$  cells/mL were tested, followed by quantification of neurite length and width again at day 5 post embedding (Figure 6). Here, the lengths  $(29.4 \pm 1.3, 27.4 \pm 1.6, 28.1 \pm 1.5 \mu m, respectively)$ and widths (3.9  $\pm$  0.2, 3.9  $\pm$  0.2, 3.8  $\pm$  0.3  $\mu$ m, respectively; Figure 6) of neurites were not significantly different in the GelMA-Cad hydrogels as a function of cell density. Thus, these results demonstrate that GelMA-Cad is an effective hydrogel for enhancing survival and maturation of the singularized human iPSC-derived neurons by morphometric parameters regardless of the initial cell seeding density.

iPSC-Derived Neurons form Synaptically Connected Networks in GelMA-Cad Hydrogels. The increased length and width of neurites in GelMA-Cad suggested that the neurons are being conferred with improved functional properties, which we sought to validate with additional metrics including immunostaining, electrophysiological recordings, and viral synaptic tracing. First, we fixed and immunostained embedded neurons for synaptophysin (a presynaptic terminal marker) and PSD-95 (a postsynaptic terminal marker). The neurons embedded in GelMA-Cad expressed both markers 21 days after embedding (average of 492 synaptophysin puncta and 423 PSD-95 puncta per 75  $\mu$ m<sup>3</sup>), and there was an average colocalization of  $87.3 \pm 1.3\%$ , which indicates the formation of active synapses (Figure 7A). The neurons embedded in Matrigel had substantially lower expression of synaptophysin and PSD-95 (average of 82 puncta and 28 puncta per 75  $\mu$ m<sup>3</sup>, respectively), with only 13.3 ± 3.3% colocalization of the presynaptic and postsynaptic markers (Figure 7A), indicating a lower number of functional synapses. Next, to initially assess synaptic connectivity, we measured the electrical activity of the embedded neurons through extracellular field potential measurements. Action potentials were readily measured within the neurons embedded in GelMA-Cad (Figure 7B, red line), but only minimal activity was observed in the Matrigelembedded neurons (Figure 7B, black line), thus providing evidence that the N-cadherin peptide improves functional maturity.

Finally, we conducted synaptic tracing experiments by transducing iPSC-derived neurons with an adeno-associated virus (AAV) encoding EGFP under the control of the human synapsin promoter (where synapsin is a presynaptic terminal marker). Wild-type neurons were mixed with the hydrogel precursor, and prior to cross-linking the hydrogels, a small population of AAV-transduced neurons (1:100 ratio of the transduced to nontransduced neurons) was injected into the center (Figure 8). The spread of the EGFP signal could thus be monitored over time to demonstrate functional synaptic connections. Limited EGFP spread was observed after 7 days, which is consistent with Figure 5, demonstrating that neurite length and width are still increasing at this early time point. However, after 21 days, EGFP had propagated to many neurons within the GelMA-Cad hydrogels, whereas sparse EGFP spread was observed in Matrigel (Figure 8). Calcein dye was added to each hydrogel to show that the neurons in Matrigel were alive but not synaptically connected. Quantification of EGFP and calcein colocalization further highlighted

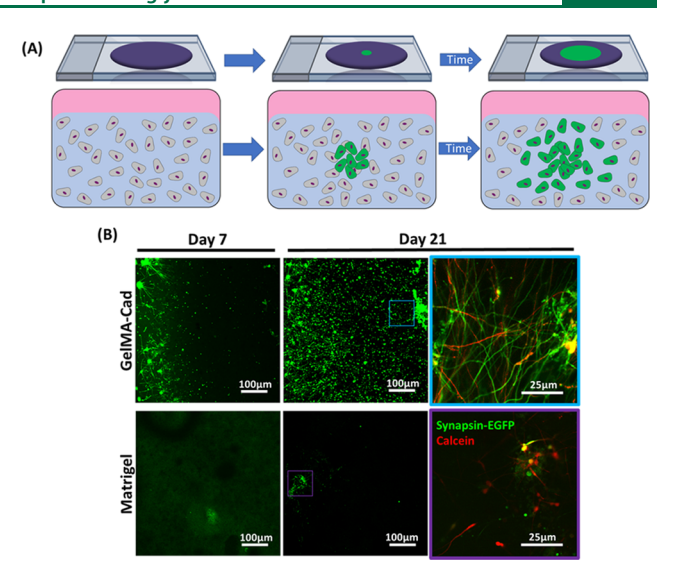


**Figure 8.** Assessment of the synaptic connectivity of the iPSC-derived neurons in Matrigel or GelMA-Cad by viral tracing. (A) Schematic depicts the experimental approach, where the wild-type neurons were uniformly mixed in a hydrogel and a small population of the AAV-transduced neurons was injected into the center. (B) Representative images of EGFP on day 7 and day 21. Calcein (red) was added on day 21 to verify cell viability and is shown in the insets. Colocalization of EGFP and calcein was quantified on day 21 in compressed z-stacks imaged across six biological replicates (1 image per replicate). A student's unpaired t-test was used to assess statistical significance.

this outcome (89  $\pm$  0.3% colocalization in GelMA-Cad versus 21  $\pm$  0.2% colocalization in Matrigel; p < 0.0001). Therefore, only the neurons in the GelMA-Cad hydrogels were able to propagate the virus through functional synapses across the entire tissue construct. Overall, these data strongly suggest that GelMA-Cad facilitates the maturation of the iPSC-derived neurons on a functional level.

## DISCUSSION

In native tissues, cells are surrounded by a complex ECM that presents both physical and biochemical cues for tissue development, migration, and proliferation.<sup>56</sup> In the brain, the neurons are encased in a soft ECM comprised of various proteins and glycosaminoglycans (GAGs). Many ECMs, as described earlier, have been tested for their ability to support 3D in vitro cultures of neural cells. Several studies have focused on the effect of ECM stiffness and composition on the differentiation of NPCs to terminally differentiated progenies, 57,58 but relatively fewer have examined functional maturation and integration of neurons, particularly those derived from hPSCs. hPSC-derived neurons are notoriously difficult to mature in two-dimensional (2D) without extended culture times or co-culture with astrocytes, 54,59 though more success has been observed in 3D assembly. 60 In particular, hydrogels comprised of methacrylated HA can facilitate the maturation of iPSC-derived neurons to an electrophysiologically active state, 18 which is perhaps unsurprising given that HA is the most abundant GAG in the brain tissue. Yet, as mentioned previously, HA has limitations that make it less attractive for either large-scale work or applications requiring patterned structures.

Our approach to these challenges was to use a relatively simple ECM material (GelMA, a well-established biomaterial known to support primary neural cells in 3D matrices<sup>35</sup>) and

append it with a biophysical cue to mimic cell-cell communication in the developing and adult brain. N-cadherin was chosen for several reasons. From a biomaterials perspective, the N-cadherin extracellular epitope had already been incorporated into HA gels and shown to be bioactive for cartilage tissue engineering, so it was straightforward to incorporate this epitope into GelMA. Moreover, tethering of an N-cadherin peptide to a solid support had previously been shown to improve neuronal survival and neurite outgrowth of stem cell-derived neurons in 2D cultures, 41,61,62 suggesting relevance for our work in 3D scaffolds. From a biochemical perspective, N-cadherin expression is important for the outgrowth of the neurites on astrocyte monolayers, and given that hPSC-derived neurons are typically cultured on 2D monolayers of astrocytes to facilitate electrophysiological maturation,<sup>63</sup> we suspected that GelMA-Cad could partially replace the synaptogenic role of astrocyte co-culture. Cadherins also regulate dendritic spine morphology<sup>64</sup> and Ncadherin-mediated interactions are specifically required for maintenance of dendrites,65 which is particularly interesting because we observed an especially pronounced increase in the expression of postsynaptic terminal markers on the neurons in GelMA-Cad relative to Matrigel. Thus, we believe that GelMA-Cad may specifically enhance synapse formation in iPSCderived neurons by facilitating postsynaptic terminal maturation. This is a key difference between the GelMA-Cad hydrogels and most other ECM-based hydrogels used for neural tissue engineering,<sup>66</sup> which typically seek to mimic key cell-ECM interactions rather than replace key cell-cell interactions.

One confounding variable in our study is that the stiffnesses of the GelMA-Cad and control hydrogels were not perfectly matched. Our rheology measurements suggest that bulk GelMA-Cad hydrogels are ~50% stiffer than the controls. These measurements contrast somewhat with the localized stiffness measurements performed by AFM, where the average stiffnesses are similar to the rheology measurements, but the differences are not statistically significant. In general, we would expect AFM to detect more subtle differences in stiffness at the nanoscale, which may be more representative of the stiffness that the neurons would sense within the hydrogel. Furthermore, because Matrigel hydrogels are softer than GelMA and GelMA-Scram (previously measured at 20-300 Pa by rheology and 443 Pa by AFM<sup>67,68</sup>), we believe that the Cad peptide has a greater impact on neuron survival and maturation compared to the hydrogel mechanics. Overall, because the stiffness of GelMA-Cad should be tunable through the degree of photopolymerization, we expect to address this limitation in future studies where hydrogel mechanics can be more similarly matched between all conditions.

It is also possible that the gelatin backbone of GelMA-Cad augments neuron health and survival. Gelatin-based hydrogels can be neuroprotective and promote neurite outgrowth through integrin activation and integrin-dependent MAPK signaling. Gelatin also improves in vivo outcomes in dissected nerve regeneration, particularly through increased axonal migration. Recent work has further shown that GelMA alone can support dissociated primary mouse neurons to create a synaptically connected neural network on the micron scale. This finding contrasts somewhat with our observations of neuron death in GelMA and GelMA-Scram. However, beyond the obvious species differences, we note that this prior study utilized neurons that had already matured in

vivo. Thus, the primary neurons may have been competent enough to form neural networks in GelMA because they already expressed the requisite synaptic machinery, rather than requiring de novo expression of this machinery in the hPSCderived neurons developing from a more embryonic-like state. Furthermore, our study utilized neurons that were enzymatically dissociated into single-cell suspensions, whereas these primary neuron suspensions were manually dissociated and therefore were likely to retain crucial cell-cell interactions during encapsulation. Our observation of ubiquitous cell death of single-cell neuron suspensions in GelMA and GelMA-Scram at lower densities  $(1 \times 10^7 \text{ cells/mL})$  in the aforementioned study<sup>72</sup> versus  $2 \times 10^5$  cells/mL in this study) supports the notion that these cell-cell interactions are key for survival. Likewise, the ability of GelMA-Cad to support the survival of the singularized neurons at low encapsulation densities, followed by robust neurite outgrowth, suggests that the peptide epitope in GelMA-Cad also supports cell adhesion and recapitulates crucial cell-cell interactions in addition to its ability to promote synaptic connectivity. It is possible that addition of other peptide epitopes, such as the wellcharacterized IKVAV found in laminin<sup>73</sup> or Arg-Gly-Asp (RGD) adhesion motifs (to augment the endogenous RGD motifs found in gelatin), could further enhance the properties of GelMA-Cad.

#### CONCLUSIONS

Overall, our work provides an exciting scaffolding material for future efforts devoted to assembling complex neurovascular tissue structures. If N-cadherin signaling is a general mechanism for synaptic integration, we speculate that multiple iPSC-derived neuronal cell types could be patterned into complex architectures that would be subsequently directed by the ECM to form relevant neural circuitry. The inclusion of iPSC-derived astrocytes and microglia could further be used to study synaptic pruning and remodeling under healthy and diseased conditions. Then, given the mechanical integrity of GelMA-Cad hydrogels, various micropatterning approaches could be used to generate perfusable channels seeded with endothelial and mural cells, ultimately resulting in functional vasculature throughout the human neural networks. The bioactivity of GelMA-Cad, coupled to its relatively low cost and ease of synthesis, should make it attractive for the aforementioned applications, as well as other situations throughout bioengineering and neuroscience.

#### ASSOCIATED CONTENT

## Supporting Information

The Supporting Information is available free of charge at https://pubs.acs.org/doi/10.1021/acsbiomaterials.0c00885.

Patterning of macrostructures in GelMA-Cad, influence of the soluble peptides on neuron viability, and influence of conjugated peptide density on the neuron physical properties (Figures S1-S3) (PDF)

## AUTHOR INFORMATION

# **Corresponding Authors**

Leon M. Bellan — Interdisciplinary Materials Science Program, Department of Biomedical Engineering, and Department of Mechanical Engineering, Vanderbilt University, Nashville, Tennessee 37235, United States; Email: leon.m.bellan@ vanderbilt.edu Ethan S. Lippmann — Department of Chemical and Biomolecular Engineering, Interdisciplinary Materials Science Program, Department of Biomedical Engineering, and Vanderbilt Brain Institute, Vanderbilt University, Nashville, Tennessee 37235, United States; Department of Neurology, Vanderbilt University Medical Center, Nashville, Tennessee 37232, United States; orcid.org/0000-0001-5703-5747; Email: ethan.s.lippmann@vanderbilt.edu

## **Authors**

- Brian J. O'Grady Department of Chemical and Biomolecular Engineering and Interdisciplinary Materials Science Program, Vanderbilt University, Nashville, Tennessee 37235, United States
- Kylie M. Balotin Department of Biomedical Engineering, Vanderbilt University, Nashville, Tennessee 37235, United States
- Allison M. Bosworth Department of Biomedical Engineering, Vanderbilt University, Nashville, Tennessee 37235, United States
- P. Mason McClatchey Department of Molecular Physiology and Biophysics, Vanderbilt University, Nashville, Tennessee 37235, United States
- Robert M. Weinstein Department of Chemical and Biomolecular Engineering and Department of Biomedical Engineering, Vanderbilt University, Nashville, Tennessee 37235, United States
- Mukesh Gupta Department of Biomedical Engineering, Vanderbilt University, Nashville, Tennessee 37235, United States
- Kara S. Poole Department of Chemical and Biomolecular Engineering, Vanderbilt University, Nashville, Tennessee 37235, United States

Complete contact information is available at: https://pubs.acs.org/10.1021/acsbiomaterials.0c00885

## **Author Contributions**

B.J.O. and K.M.B. are co-first authors and L.M.B. and E.S.L. are co-senior authors.

#### **Notes**

The authors declare the following competing financial interest(s): Several authors on this manuscript have filed a patent application on the GelMA-Cad biomaterial.

## ACKNOWLEDGMENTS

The authors would like to thank Dr. Anthony Hmelo and the Vanderbilt Institute of Nanoscale Science and Engineering (VINSE) for assistance with atomic force microscopy and scanning electron microscopy. The authors would also like to thank Dr. Laura Dugan and Jacob Ruden for the use of electrophysiology equipment. Funding for this work was provided by a Ben Barres Early Career Acceleration Award from the Chan Zuckerberg Initiative (grant 2018-191850 to E.S.L.), NSF grants 1846860 and 1706155 (to E.S.L.), NSF grants 1506717 and 1462866 (to L.M.B.), a NARSAD Young Investigator Award from the Brain and Behavior Research Foundation (grant 25177 to E.S.L.), the donors of Alzheimer's Disease Research, which is a program of the BrightFocus Foundation (grant A20170945 to E.S.L.), and NIH grants R00EB013630 (to L.M.B.), R01NS110665 (to E.S.L.), and 5P30DK020593 (pilot award to E.S.L.). B.J.O. was partially supported by the NIH-funded Vanderbilt Interdisciplinary

Training Program in Alzheimer's Disease (T32AG058524). K.M.B. was partially supported by the NIH-funded Training Program in Environmental Toxicology (T32ES007028). P.M.M. was supported by an NIH NRSA fellowship (F32DK120104).

#### REFERENCES

- (1) Vanni, S.; Baldeschi, A. C.; Zattoni, M.; Legname, G. Brain Aging: A Ianus-Faced Player between Health and Neurodegeneration. *J. Neurosci. Res.* **2019**, *98*, 299–311.
- (2) Mehta, D.; Jackson, R.; Paul, G.; Shi, J.; Sabbagh, M. Why Do Trials for Alzheimer's Disease Drugs Keep Failing? A Discontinued Drug Perspective for 2010-2015. *Expert Opin. Invest. Drugs* **2017**, 26, 735–739.
- (3) Denayer, T.; Stöhr, T.; Roy, M. V. Animal Models in Translational Medicine: Validation and Prediction. *Eur. J. Mol. Clin. Med.* **2014**, *2*, 5–11.
- (4) Bolker, J. A. Animal Models in Translational Research: Rosetta Stone or Stumbling Block? *BioEssays* **2017**, *39*, No. 1700089.
- (5) Zhang, D.; Pekkanen-Mattila, M.; Shahsavani, M.; Falk, A.; Teixeira, A. I.; Herland, A. A 3D Alzheimer's Disease Culture Model and the Induction of P21-Activated Kinase Mediated Sensing in IPSC Derived Neurons. *Biomaterials* **2014**, *35*, 1420–1428.
- (6) Tian, X.-F.; Heng, B.-C.; Ge, Z.; Lu, K.; Rufaihah, A. J.; Fan, V. T.-W.; Yeo, J.-F.; Cao, T. Comparison of Osteogenesis of Human Embryonic Stem Cells within 2D and 3D Culture Systems. *Scand. J. Clin. Lab. Invest.* **2008**, *68*, 58–67.
- (7) Imamura, Y.; Mukohara, T.; Shimono, Y.; Funakoshi, Y.; Chayahara, N.; Toyoda, M.; Kiyota, N.; Takao, S.; Kono, S.; Nakatsura, T.; Minami, H. Comparison of 2D- and 3D-Culture Models as Drug-Testing Platforms in Breast Cancer. *Oncol. Rep.* **2015**, 33, 1837–1843.
- (8) Zhuang, P.; Sun, A. X.; An, J.; Chua, C. K.; Chew, S. Y. 3D Neural Tissue Models: From Spheroids to Bioprinting. *Biomaterials* **2018**, *154*, 113–133.
- (9) Lancaster, M. A.; Renner, M.; Martin, C.-A.; Wenzel, D.; Bicknell, L. S.; Hurles, M. E.; Homfray, T.; Penninger, J. M.; Jackson, A. P.; Knoblich, J. A. Cerebral Organoids Model Human Brain Development and Microcephaly. *Nature* **2013**, *501*, 373–379.
- (10) Di Lullo, E.; Kriegstein, A. R. The Use of Brain Organoids to Investigate Neural Development and Disease. *Nat. Rev. Neurosci.* **2017**, *18*, 573–584.
- (11) Long, K. R.; Huttner, W. B. How the Extracellular Matrix Shapes Neural Development; Royal Society Publishing: 2019; Vol. 9.
- (12) Hughes, C. S.; Postovit, L. M.; Lajoie, G. A. Matrigel: A Complex Protein Mixture Required for Optimal Growth of Cell Culture. *Proteomics* **2010**, *10*, 1886–1890.
- (13) Kothapalli, C. R.; Kamm, R. D. 3D Matrix Microenvironment for Targeted Differentiation of Embryonic Stem Cells into Neural and Glial Lineages. *Biomaterials* **2013**, *34*, 5995–6007.
- (14) Fatehullah, A.; Tan, S. H.; Barker, N. Organoids as an in Vitro Model of Human Development and Disease. *Nat. Cell Biol.* **2016**, *18*, 246–254.
- (15) Wang, H. Modeling Neurological Diseases With Human Brain Organoids. Front. Synaptic Neurosci. 2018, 10, No. 15.
- (16) Cantley, W. L.; Du, C.; Lomoio, S.; DePalma, T.; Peirent, E.; Kleinknecht, D.; Hunter, M.; Tang-Schomer, M. D.; Tesco, G.; Kaplan, D. L. Functional and Sustainable 3D Human Neural Network Models from Pluripotent Stem Cells. ACS Biomater Sci Eng 2018, 4, 4278–4288.
- (17) Pietrucha, K.; Zychowicz, M.; Podobinska, M.; Buzanska, L. Functional Properties of Different Collagen Scaffolds to Create a Biomimetic Niche for Neurally Committed Human Induced Pluripotent Stem Cells (IPSC). *Folia Neuropathol.* **2017**, *2*, 110–123. (18) Zhang, Z.-N.; Freitas, B. C.; Qian, H.; Lux, J.; Acab, A.; Trujillo, C. A.; Herai, R. H.; Huu, V. A. N.; Wen, J. H.; Joshi-Barr, S.; Karpiak, J. V.; Engler, A. J.; Fu, X.-D.; Muotri, A. R.; Almutairi, A. Layered Hydrogels Accelerate IPSC-Derived Neuronal Maturation and Reveal

- Migration Defects Caused by MeCP2 Dysfunction. *Proc. Natl. Acad. Sci. U.S.A.* **2016**, *113*, 3185–3190.
- (19) Barry, C.; Schmitz, M. T.; Propson, N. E.; Hou, Z.; Zhang, J.; Nguyen, B. K.; Bolin, J. M.; Jiang, P.; McIntosh, B. E.; Probasco, M. D.; Swanson, S.; Stewart, R.; Thomson, J. A.; Schwartz, M. P.; Murphy, W. L. Uniform Neural Tissue Models Produced on Synthetic Hydrogels Using Standard Culture Techniques. *Exp. Biol. Med.* **2017**, 242, 1679–1689.
- (20) Madl, C. M.; LeSavage, B. L.; Dewi, R. E.; Dinh, C. B.; Stowers, R. S.; Khariton, M.; Lampe, K. J.; Nguyen, D.; Chaudhuri, O.; Enejder, A.; Heilshorn, S. C. Maintenance of Neural Progenitor Cell Stemness in 3D Hydrogels Requires Matrix Remodelling. *Nat. Mater.* 2017, 16, 1233–1242.
- (21) Oksdath, M.; Perrin, S. L.; Bardy, C.; Hilder, E. F.; DeForest, C. A.; Arrua, R. D.; Gomez, G. A. Review: Synthetic Scaffolds to Control the Biochemical, Mechanical, and Geometrical Environment of Stem Cell-Derived Brain Organoids. *APL Bioeng.* **2018**, *2*, No. 041501.
- (22) Klotz, B. J.; Gawlitta, D.; Rosenberg, A. J. W. P.; Malda, J.; Melchels, F. P. W. Gelatin-Methacryloyl Hydrogels: Towards Biofabrication-Based Tissue Repair. *Trends Biotechnol.* **2016**, *34*, 394–407.
- (23) Köhler, P.; Wolff, A.; Ejserholm, F.; Wallman, L.; Schouenborg, J.; Linsmeier, C. E. Influence of Probe Flexibility and Gelatin Embedding on Neuronal Density and Glial Responses to Brain Implants. *PLoS One* **2015**, *10*, No. e0119340.
- (24) Georgiou, M.; Bunting, S. C. J.; Davies, H. A.; Loughlin, A. J.; Golding, J. P.; Phillips, J. B. Engineered Neural Tissue for Peripheral Nerve Repair. *Biomaterials* **2013**, *34*, 7335–7343.
- (25) Chwalek, K.; Sood, D.; Cantley, W. L.; White, J. D.; Tang-Schomer, M.; Kaplan, D. L. Engineered 3D Silk-Collagen-Based Model of Polarized Neural Tissue. *J. Visualized Exp.* **2015**, *104*, No. e52970.
- (26) Zhu, J.; Marchant, R. E. Design Properties of Hydrogel Tissue-Engineering Scaffolds. *Expert Rev. Med. Devices* **2011**, *8*, 607–626.
- (27) Zhou, X.; Cui, H.; Nowicki, M.; Miao, S.; Lee, S. J.; Masood, F.; Harris, B. T.; Zhang, L. G. Three-Dimensional-Bioprinted Dopamine-Based Matrix for Promoting Neural Regeneration. *ACS Appl. Mater. Interfaces* **2018**, *10*, 8993–9001.
- (28) Davey, S. K.; Aung, A.; Agrawal, G.; Lim, H. L.; Kar, M.; Varghese, S. Embedded 3D Photopatterning of Hydrogels with Diverse and Complex Architectures for Tissue Engineering and Disease Models. *Tissue Eng., Part C* 2015, 21, 1188–1196.
- (29) Nichol, J. W.; Koshy, S. T.; Bae, H.; Hwang, C. M.; Yamanlar, S.; Khademhosseini, A. Cell-Laden Microengineered Gelatin Methacrylate Hydrogels. *Biomaterials* **2010**, *31*, 5536–5544.
- (30) Bian, L.; Guvendiren, M.; Mauck, R. L.; Burdick, J. A. Hydrogels That Mimic Developmentally Relevant Matrix and N-Cadherin Interactions Enhance MSC Chondrogenesis. *Proc. Natl. Acad. Sci. U.S.A.* **2013**, *110*, 10117–10122.
- (31) Kumar, K. K.; Lowe, J. E. W.; Aboud, A. A.; Neely, M. D.; Redha, R.; Bauer, J. A.; Odak, M.; Weaver, C. D.; Meiler, J.; Aschner, M.; Bowman, A. B. Cellular Manganese Content Is Developmentally Regulated in Human Dopaminergic Neurons. *Sci. Rep.* **2015**, *4*, No. 6801.
- (32) Lippmann, E. S.; Estevez-Silva, M. C.; Ashton, R. S. Defined Human Pluripotent Stem Cell Culture Enables Highly Efficient Neuroepithelium Derivation Without Small Molecule Inhibitors. *Stem Cells* **2014**, 32, 1032–1042.
- (33) Shi, Y.; Kirwan, P.; Livesey, F. J. Directed Differentiation of Human Pluripotent Stem Cells to Cerebral Cortex Neurons and Neural Networks. *Nat. Protoc.* **2012**, *7*, 1836–1846.
- (34) Chambers, S. M.; Fasano, C. A.; Papapetrou, E. P.; Tomishima, M.; Sadelain, M.; Studer, L. Highly Efficient Neural Conversion of Human ES and IPS Cells by Dual Inhibition of SMAD Signaling. *Nat. Biotechnol.* **2009**, *27*, 275–280.
- (35) Loessner, D.; Meinert, C.; Kaemmerer, E.; Martine, L. C.; Yue, K.; Levett, P. A.; Klein, T. J.; Melchels, F. P. W.; Khademhosseini, A.; Hutmacher, D. W. Functionalization, Preparation and Use of Cell-

- Laden Gelatin Methacryloyl-Based Hydrogels as Modular Tissue Culture Platforms. *Nat. Protoc.* **2016**, *11*, 727–746.
- (36) Li, X.; Chen, S.; Li, J.; Wang, X.; Zhang, J.; Kawazoe, N.; Chen, G. 3D Culture of Chondrocytes in Gelatin Hydrogels with Different Stiffness. *Polymers* **2016**, *8*, No. 269.
- (37) Lee, B. H.; Lum, N.; Seow, L. Y.; Lim, P. Q.; Tan, L. P. Synthesis and Characterization of Types A and B Gelatin Methacryloyl for Bioink Applications. *Materials* **2016**, *9*, No. 797.
- (38) Stroka, K. M.; Aranda-Espinoza, H. Endothelial Cell Substrate Stiffness Influences Neutrophil Transmigration via Myosin Light Chain Kinase-Dependent Cell Contraction. *Blood* **2011**, *118*, 1632—1640.
- (39) McClatchey, P. M.; Mignemi, N. A.; Xu, Z.; Williams, I. M.; Reusch, J. E. B.; McGuinness, O. P.; Wasserman, D. H. Automated Quantification of Microvascular Perfusion. *Microcirculation* **2018**, 25, No. e12482.
- (40) McClatchey, P. M.; Keller, A. C.; Bouchard, R.; Knaub, L. A.; Reusch, J. E. B. Fully Automated Software for Quantitative Measurements of Mitochondrial Morphology. *Mitochondrion* **2016**, 26, 58–71.
- (41) Haque, A.; Adnan, N.; Motazedian, A.; Akter, F.; Hossain, S.; Kutsuzawa, K.; Nag, K.; Kobatake, E.; Akaike, T. An Engineered N-Cadherin Substrate for Differentiation, Survival, and Selection of Pluripotent Stem Cell-Derived Neural Progenitors. *PLoS One* **2015**, *10*. No. e0135170.
- (42) Kadowaki, M.; Nakamura, S.; Machon, O.; Krauss, S.; Radice, G. L.; Takeichi, M. N-Cadherin Mediates Cortical Organization in the Mouse Brain. *Dev. Biol.* **2007**, *304*, 22–33.
- (43) Jontes, J. D. The Cadherin Superfamily in Neural Circuit Assembly. *Cold Spring Harb Perspect. Biol.* **2018**, *10*, No. a029306.
- (44) Xu, C.; Funahashi, Y.; Watanabe, T.; Takano, T.; Nakamuta, S.; Namba, T.; Kaibuchi, K. Radial Glial Cell—Neuron Interaction Directs Axon Formation at the Opposite Side of the Neuron from the Contact Site. *J. Neurosci.* **2015**, *35*, 14517–14532.
- (45) Shikanai, M.; Nakajima, K.; Kawauchi, T. N-Cadherin Regulates Radial Glial Fiber-Dependent Migration of Cortical Locomoting Neurons. *Commun. Integr. Biol.* **2011**, *4*, 326–330.
- (46) Matsunaga, Y.; Noda, M.; Murakawa, H.; Hayashi, K.; Nagasaka, A.; Inoue, S.; Miyata, T.; Miura, T.; Kubo, K.; Nakajima, K. Reelin Transiently Promotes N-Cadherin—Dependent Neuronal Adhesion during Mouse Cortical Development. *Proc. Natl. Acad. Sci. U.S.A.* **2017**, *114*, 2048–2053.
- (47) Yue, K.; Trujillo-de Santiago, G.; Alvarez, M. M.; Tamayol, A.; Annabi, N.; Khademhosseini, A. Synthesis, Properties, and Biomedical Applications of Gelatin Methacryloyl (GelMA) Hydrogels. *Biomaterials* **2015**, *73*, 254–271.
- (48) Miller, K.; Chinzei, K.; Orssengo, G.; Bednarz, P. Mechanical Properties of Brain Tissue In-Vivo: Experiment and Computer Simulation. *J. Biomech.* **2000**, *33*, 1369–1376.
- (49) Hirakawa, K.; Hashizume, K.; Hayashi, T. Viscoelastic Property of Human Brain -for the Analysis of Impact Injury (Author's Transl). *No To Shinkei* **1981**, *33*, 1057–1065.
- (50) Bertassoni, L. E.; Cecconi, M.; Manoharan, V.; Nikkhah, M.; Hjortnaes, J.; Cristino, A. L.; Barabaschi, G.; Demarchi, D.; Dokmeci, M. R.; Yang, Y.; Khademhosseini, A. Hydrogel Bioprinted Microchannel Networks for Vascularization of Tissue Engineering Constructs. *Lab Chip* **2014**, *14*, 2202–2211.
- (51) Meijering, E. Neuron Tracing in Perspective. *Cytometry, Part A* **2010**, 77A, 693–704.
- (52) Ascoli, G. A. Neuroinformatics Grand Challenges. *Neuroinformatics* **2008**, *6*, 1–3.
- (53) Radio, N. M.; Mundy, W. R. Developmental Neurotoxicity Testing in Vitro: Models for Assessing Chemical Effects on Neurite Outgrowth. *NeuroToxicology* **2008**, *29*, 361–376.
- (54) Odawara, A.; Katoh, H.; Matsuda, N.; Suzuki, I. Physiological Maturation and Drug Responses of Human Induced Pluripotent Stem Cell-Derived Cortical Neuronal Networks in Long-Term Culture. *Sci. Rep.* **2016**, *6*, No. 26181.

- (55) Winans, A. M.; Collins, S. R.; Meyer, T. Waves of Actin and Microtubule Polymerization Drive Microtubule-Based Transport and Neurite Growth before Single Axon Formation. *eLife* **2016**, *S*, No. e12387.
- (56) Muncie, J. M.; Weaver, V. M. The Physical and Biochemical Properties of the Extracellular Matrix Regulate Cell Fate. *Curr. Top. Dev. Biol.* **2018**, *130*, 1–37.
- (57) Keung, A. J.; Dong, M.; Schaffer, D. V.; Kumar, S. Pan-Neuronal Maturation but Not Neuronal Subtype Differentiation of Adult Neural Stem Cells Is Mechanosensitive. *Sci. Rep.* **2013**, *3*, No. 1817.
- (58) Keung, A. J.; Juan-Pardo, E. M.; de Schaffer, D. V.; Kumar, S. Rho GTPases Mediate the Mechanosensitive Lineage Commitment of Neural Stem Cells. *Stem Cells* **2011**, *29*, 1886–1897.
- (59) Hedegaard, A.; Monzón-Sandoval, J.; Newey, S. E.; Whiteley, E. S.; Webber, C.; Akerman, C. J. Pro-Maturational Effects of Human IPSC-Derived Cortical Astrocytes upon IPSC-Derived Cortical Neurons. *Stem Cell Rev.* **2020**, *15*, 38–51.
- (60) Paşca, A. M.; Sloan, S. A.; Clarke, L. E.; Tian, Y.; Makinson, C. D.; Huber, N.; Kim, C. H.; Park, J.-Y.; O'Rourke, N. A.; Nguyen, K. D.; Smith, S. J.; Huguenard, J. R.; Geschwind, D. H.; Barres, B. A.; Paşca, S. P. Functional Cortical Neurons and Astrocytes from Human Pluripotent Stem Cells in 3D Culture. *Nat. Methods* **2015**, *12*, 671–678.
- (61) Lim, H. J.; Khan, Z.; Wilems, T. S.; Lu, X.; Perera, T. H.; Kurosu, Y. E.; Ravivarapu, K. T.; Mosley, M. C.; Smith Callahan, L. A. Human Induced Pluripotent Stem Cell Derived Neural Stem Cell Survival and Neural Differentiation on Polyethylene Glycol Dimethacrylate Hydrogels Containing a Continuous Concentration Gradient of N-Cadherin Derived Peptide His-Ala-Val-Asp-Ile. ACS Biomater. Sci. Eng. 2017, 3, 776–781.
- (62) Cherry, J. F.; Bennett, N. K.; Schachner, M.; Moghe, P. V. Engineered N-Cadherin and L1 Biomimetic Substrates Concertedly Promote Neuronal Differentiation, Neurite Extension and Neuroprotection of Human Neural Stem Cells. *Acta Biomater.* **2014**, *10*, 4113–4126.
- (63) Tomaselli, K. J.; Neugebauer, K. M.; Bixby, J. L.; Lilien, J.; Reichard, L. F. N-Cadherin and Integrins: Two Receptor Systems That Mediate Neuronal Process Outgrowth on Astrocyte Surfaces. *Neuron* 1988, 1, 33–43.
- (64) Togashi, H.; Abe, K.; Mizoguchi, A.; Takaoka, K.; Chisaka, O.; Takeichi, M. Cadherin Regulates Dendritic Spine Morphogenesis. *Neuron* **2002**, *35*, 77–89.
- (65) Tan, Z. J.; Peng, Y.; Song, H. L.; Zheng, J. J.; Yu, X. N-Cadherin-Dependent Neuron-Neuron Interaction Is Required for the Maintenance of Activity-Induced Dendrite Growth. *Proc. Natl. Acad. Sci. U.S.A.* **2010**, *107*, 9873–9878.
- (66) Boni, R.; Ali, A.; Shavandi, A.; Clarkson, A. N. Current and Novel Polymeric Biomaterials for Neural Tissue Engineering. *J. Biomed. Sci.* **2018**, 25, No. 90.
- (67) Chaudhuri, O.; Koshy, S. T.; Branco da Cunha, C.; Shin, J.-W.; Verbeke, C. S.; Allison, K. H.; Mooney, D. J. Extracellular Matrix Stiffness and Composition Jointly Regulate the Induction of Malignant Phenotypes in Mammary Epithelium. *Nat. Mater.* **2014**, *13*, 970–978.
- (68) Soofi, S. S.; Last, J. A.; Liliensiek, S. J.; Nealey, P. F.; Murphy, C. J. The Elastic Modulus of Matrigel as Determined by Atomic Force Microscopy. *J. Struct. Biol.* **2009**, *167*, 216–219.
- (69) Du, B. L.; Zeng, C. G.; Zhang, W.; Quan, D. P.; Ling, E. A.; Zeng, Y. S. A Comparative Study of Gelatin Sponge Scaffolds and PLGA Scaffolds Transplanted to Completely Transected Spinal Cord of Rat. J. Biomed. Mater. Res., Part A 2014, 102, 1715–1725.
- (70) Li, G.; Che, M.-T.; Zhang, K.; Qin, L.-N.; Zhang, Y.-T.; Chen, R.-Q.; Rong, L.-M.; Liu, S.; Ding, Y.; Shen, H.-Y.; Long, S.-M.; Wu, J.-L.; Ling, E.-A.; Zeng, Y.-S. Graft of the NT-3 Persistent Delivery Gelatin Sponge Scaffold Promotes Axon Regeneration, Attenuates Inflammation, and Induces Cell Migration in Rat and Canine with Spinal Cord Injury. *Biomaterials* **2016**, *83*, 233–248.

- (71) Liu, S.; Sun, X.; Wang, T.; Chen, S.; Zeng, C.-G.; Xie, G.; Zhu, Q.; Liu, X.; Quan, D. Nano-Fibrous and Ladder-like Multi-Channel Nerve Conduits: Degradation and Modification by Gelatin. *Mater. Sci. Eng.: C* **2018**, 83, 130–142.
- (72) Ren, T.; Grosshäuser, B.; Sridhar, K.; Nieland, T. J. F.; Tocchio, A.; Schepers, U.; Demirci, U. 3-D Geometry and Irregular Connectivity Dictate Neuronal Firing in Frequency Domain and Synchronization. *Biomaterials* **2019**, *197*, 171–181.
- (73) Patel, R.; Santhosh, M.; Dash, J. K.; Karpoormath, R.; Jha, A.; Kwak, J.; Patel, M.; Kim, J. H. Ile-Lys-Val-Ala-Val (IKVAV) Peptide for Neuronal Tissue Engineering. *Polym. Adv. Technol.* **2019**, *30*, 4–12.